NIMROD: The Near and InterMediate Range Order Diffractometer of the ISIS second target station

D. T. Bowron,[1,a)] A. K. Soper,[1] K. Jones,[1] S. Ansell,[1] S. Birch,[1] J. Norris,[1] L. Perrott,[1] D. Riedel,[1] N. J. Rhodes,[1] S. R. Wakefield,[1] A. Botti,[2] M.-A. Ricci,[2] F. Grazzi,[3] and M. Zoppi[3]

[1]*ISIS Facility, Rutherford Appleton Laboratory, Chilton, Didcot, Oxon OX11 0QX, United Kingdom*
[2]*Dipartimento di Fisica "E. Amaldi," Universita degli Studi Roma Tre, Via della Vasca Navale 84, 00146 Roma, Italy*
[3]*Consiglio Nazionale delle Ricerche, Istituto dei Sistemi Complessi, Via Madonna del Piano 10, I-50019 Sesto Fiorentino, Italy*

(Received 22 January 2010; accepted 2 February 2010; published online 12 March 2010)

NIMROD is the Near and InterMediate Range Order Diffractometer of the ISIS second target station. Its design is optimized for structural studies of disordered materials and liquids on a continuous length scale that extends from the atomic, upward of 30 nm, while maintaining subatomic distance resolution. This capability is achieved by matching a low and wider angle array of high efficiency neutron scintillation detectors to the broad band-pass radiation delivered by a hybrid liquid water and liquid hydrogen neutron moderator assembly. The capabilities of the instrument bridge the gap between conventional small angle neutron scattering and wide angle diffraction through the use of a common calibration procedure for the entire length scale. This allows the instrument to obtain information on nanoscale systems and processes that are quantitatively linked to the local atomic and molecular order of the materials under investigation. © *2010 American Institute of Physics.* [doi:10.1063/1.3331655]

I. INTRODUCTION

The ISIS second target station is a 10 Hz spallation neutron source that delivers a highly optimized neutron target and moderator configuration. The 100 ms time frame between neutron pulses allows the delivery of neutrons over a broad spectral range, typically with wavelengths in the range 0.04 to >12 Å, with a significantly enhanced long wavelength flux compared to that delivered from the facility's 50 Hz high power target station. This development has enabled the construction of a new generation of instrumentation that typically offers order of magnitude gains in performance for the study of nanoscale structure and phenomena.

The Near and InterMediate Range Order Diffractometer (NIMROD) is designed to capitalize on the capabilities of this new target station, to deliver a unique opportunity to study the structure of liquids and disordered and nanostructured materials in a single measurement over a continuous length scale that ranges from <1 to >300 Å, i.e., from the quantum world of atoms to the classical world of mesoscopic objects. Furthermore, through the adoption of a common calibration procedure over this entire range, the resulting data are fully quantitative. Figure 1 shows an overview of the instrument highlighting the main components in its design.

To maximize the utility of this instrument for the investigation of organic and light element containing systems, the diffractometer uses a forward scattering geometry to minimize inelastic scattering effects[1] while making use of high energy, short wavelength neutrons to deliver very high structural resolution, of the order of ~0.1 Å. This makes the instrument ideal for the performance of hydrogen-deuterium isotopic substitution experiments[2,3] that are a principal strength of the neutron scattering method.

NIMROD class diffractometers are designed to measure the interference differential scattering cross section, or total structure factor $F(Q)$, of a liquid or structurally disordered sample. Q is the magnitude of the momentum transfer vector of a scattered neutron and is defined as

$$Q = \frac{4\pi}{\lambda}\sin\theta. \tag{1}$$

λ is the wavelength of the incident neutron and 2θ is the scattering angle. In terms of this variable, $F(Q)$ is defined as

$$F(Q) = \sum_{\alpha\leq\beta} (2-\delta_{\alpha\beta}) c_\alpha c_\beta b_\alpha b_\beta [S_{\alpha\beta}(Q)-1]. \tag{2}$$

c_α and c_β are the concentrations of atom types α and β in the sample, and b_α and b_β are their corresponding neutron scattering lengths.[4] $S_{\alpha\beta}(Q)$ are the partial structure factors corresponding to the pairwise correlations between atoms of type α and β, and $\delta_{\alpha\beta}$ is the Kronecker delta function to avoid double counting interactions between like-atom pairs.

The total structure factor can be inverted to the total radial distribution function $g(r)$ by the well known Fourier transform weighted by the atomic density ρ of the system[5]

$$g(r)-1 = \frac{1}{(2\pi)^3\rho}\int_0^\infty 4\pi Q^2 F(Q)\frac{\sin Qr}{Qr}dQ. \tag{3}$$

It is the upper limit on the integral in this Fourier transform that governs the structural resolution of the resulting radial distribution function, and hence the ability of a diffractometer to measure to large values of Q is a critical require-

a)Electronic mail: daniel.bowron@stfc.ac.uk.

 © 2010 American Institute of Physics

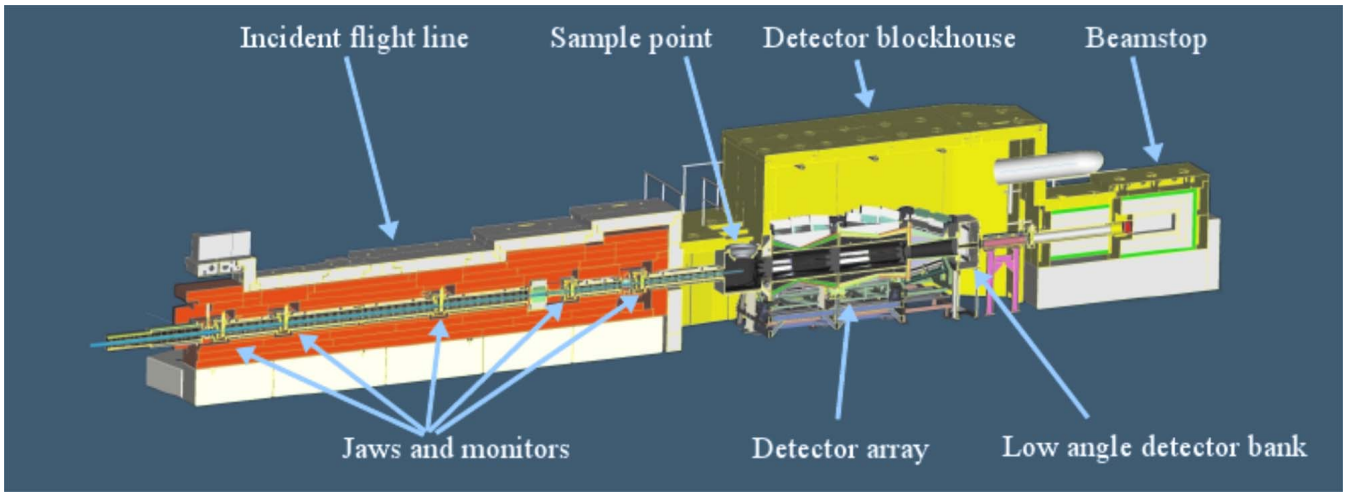

FIG. 1. (Color online) Cutaway diagram of NIMROD giving an overview of the key components from which it is constructed.

ment for high structural resolution. Formally, one can consider the structural resolution in the Fourier inverted experimental data to be given by $\pi/Q_{\max}$, so for a diffractometer to achieve a structural resolution of 0.1 Å, a $Q_{\max}$ of at least 31 Å^{-1} must be achieved.

Conversely, the requirement for the diffractometer to measure large correlation lengths imposes a requirement for the instrument to measure to small values of Q. Substituting Bragg's law into Eq. (1) shows the relationship between the magnitude of the scattering vector Q and the lattice spacing d in a crystalline material to be $Q=2\pi/d$. On this basis, if a correlation length of 300 Å is to be probed on a diffractometer, the instrument must be able to measure to a $Q_{\min}$ of at least 0.02 Å^{-1}.

It is precisely these two requirements that match the construction of NIMROD to the characteristics of the ISIS second target station. The broad spectral range of the target station enables the short wavelength neutrons to be used to access high-Q and high structural resolution, while the long wavelength neutrons are the optimal means to access low-Q and the long length scale structural correlations.

As the primary aim of the instrument is to correlate short range structure on interatomic and intermolecular length scales with nanoscale structure, the radial distribution function $g(r)$ is generally not the most ideal function to illustrate the r-space correlations. A more useful function to generate, which will be used in the later examples, is the differential pair correlation function $D(r)$.[5] This function emphasizes the long range correlations by weighting them by the length scale on which they occur, without masking the short range structure.

$$D(r) = 4\pi\rho r[g(r) - 1]. \tag{4}$$

II. INSTRUMENT COMPONENTS

A. Neutron source

NIMROD is built on port W7 of the ISIS second target station. This port views the hydrogen face of the coupled cold moderator. The moderator contains two compartments; the first is filled with solid methane that provides a grooved moderator face to ports E1–E5. This methane filled compartment backs against the second moderator volume, filled with liquid hydrogen at ≈17 K. The hydrogen face viewed by NIMROD has dimensions of 11.5 cm (height) × 12.0 cm (width). To improve the neutronic coupling of the cold moderator to the target, it is surrounded by a water filled premoderator. Early in the design phase of NIMROD, it was realized that a significant flux advantage could be gained in the short wavelength region if this premoderator was viewed as well as the methane/hydrogen moderators. The result is that a total neutron source size of 11.5 cm (height) × 19.5 cm (width) can be viewed by the sample. When combined with the 10 Hz operation of the target station and the selected incident and scattered beam flight paths on the instrument, this moderator and premoderator configuration delivers usable neutrons in the wavelength range from 0.04 to 10 Å. Figure 2 shows a schematic diagram of the moderator and premoderator configuration viewed by NIMROD and Fig. 3 shows the resulting time-of-flight neutron spectrum.

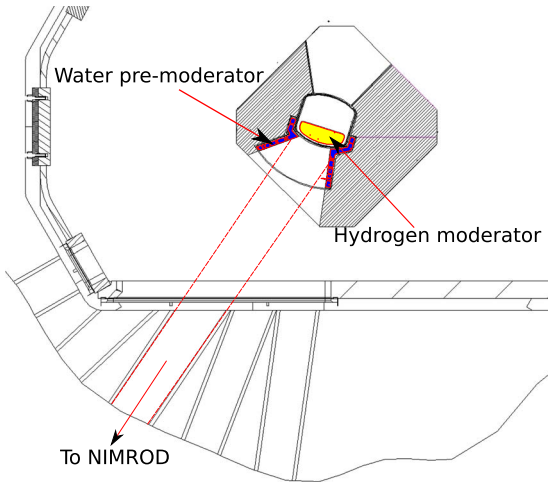

FIG. 2. (Color online) Schematic diagram of the ISIS second target station hydrogen moderator and water premoderator viewed by NIMROD.

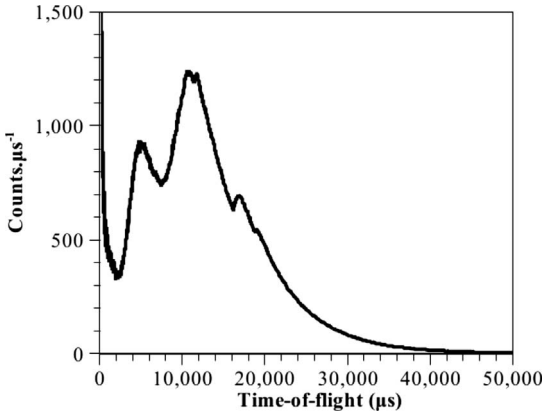

FIG. 3. Time-of-flight neutron spectrum measured on NIMROD using an incident beam monitor placed 15.26 m from the moderator face. The two peaks in the spectrum correspond to neutrons delivered from the water premoderator and the hydrogen moderator. At this monitor position, the water spectrum peaks at ~4900 μs (~1.3 Å) and the hydrogen spectrum at ~10 800 μs (~2.9 Å). The sharp features on the long wavelength side of the main peak are due to Bragg edges resulting from the scattering from the aluminum windows in the primary beam path as the neutrons exit the target station. These data were collected over a measurement time of ≈1.25 h.

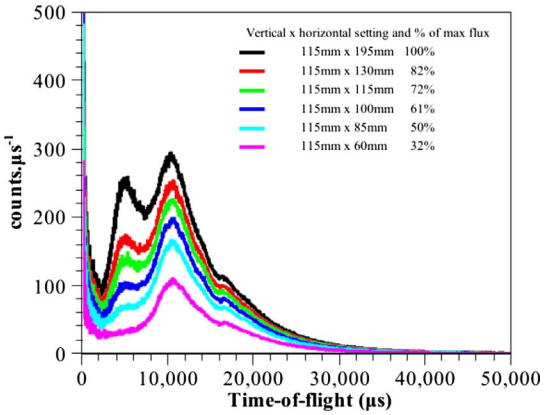

FIG. 4. (Color online) Time-of-flight neutron spectrum measured as a function of moderator and premoderator view. As the horizontal setting of the variable beam collimating jaws is changed to restrict the view of the premoderator, the spectral shape can be seen to change from the double Maxwellian profile characteristic of the combination of the water and hydrogen spectra to a single Maxwellian profile characteristic of the hydrogen moderator alone. Each set of data were collected over a measurement time of ≈0.5 h.

B. Incident neutron flight path

As the scientific aims of the instrument require the delivery of epithermal, thermal, and cold neutrons (1 meV $<E<30\,000$ meV) to the sample in every neutron pulse, as well as stringent control of the incident beam divergence, the use of a neutron guide in the primary flight path (to increase neutron flux at the sample) is not a practical option for NIMROD. Guides are ineffective for the mission critical shorter wavelength neutrons <0.3 Å that are required for access to high-Q, and also tend to increase the divergence of the beam at the sample position and so limit the small angle scattering performance. Instead, a tapering collimated neutron flight path was found to be the optimal solution for this class of instrument. To keep the intrinsic beam divergence to a manageable level for small angle scattering measurements, the incident flight path from moderator face to sample is set to 20.0 m. Over this distance, the view of the moderator face is collimated to deliver a maximum beam cross section of 3 $\times$3 cm^2 to the sample point. Fine control of the beam characteristics is achieved by means of a series of six sets of motorized collimating jaws positioned along the flight line. Measuring from the face of the moderator these are placed at 6.458, 8.072, 12.072, 15.450, 17.235, and 19.700 m. The final set is 30 cm before the sample and acts as a beam scraper to clean up the residual beam penumbra before the sample. As the configuration of these jaws elements allows them to act as variable collimation within the constraints of the main fixed collimation, the material from which they are constructed needs to be able to deal with the full range of neutron energies delivered from the target station. To this end, the blades of the three sets of jaws closest to the target station consist of 1 cm of nimonic alloy[6] (facing the moderator) backed by 1 cm of sintered boron carbide (B_4C). The nimonic alloy acts to scatter the high energy neutrons and reduce their energy while the B_4C works to absorb the thermal and cold neutrons. As nimonic alloy scatters neutrons very strongly, the blades of the three jaw sets closest to the sample are formed from 2 cm of sintered B_4C only to reduce any risk of neutrons shining off the collimating elements into the detector area. These variable collimating elements consequently provide an effective means of reducing the beam size delivered to the sample from the maximum permitted 3 $\times$3 cm^2 cross section, while also giving the instrument scientist the ability to restrict the view of the moderator face to a subsection of the 11.5$\times$19.5 cm^2 view. This allows the spectral contribution of the water premoderator to be removed from the samples view, if required, and also gives further control of the effective resolution of the diffractometer by reducing the divergence on the incident neutron beam. Figure 4 shows the effect of controlling the view of the moderator face on the flux profile delivered to the sample.

For diagnostic and data normalization purposes, a neutron beam monitor is positioned immediately after each of the first five sets of jaws in the primary flight line. Each of these monitors consists of a thin vanadium scattering foil that intercepts the full cross section of the beam profile and that is angled to scatter a small fraction of the beam into a GS20 glass scintillator[7] viewed by a photomultiplier tube.

C. Sample and secondary flight path vacuum tank

Figure 5 shows the large vacuum vessel that sits at the heart of the instrument and that serves to remove parasitic air-scattering from around the sample position and from the secondary neutron flight path. This issue is extremely important to minimize sample dependent background scattering that would otherwise contaminate the measured diffraction patterns and that is effectively impossible to correct in the data analysis procedures. The design of the vacuum tank is optimized to provide the maximum solid angle for detector coverage in the forward scattering geometry where the scattering angle 2θ varies from 0.5° to 40°. Figure 6 shows the view of the detector windows from the sample position, and illustrates how obstructions to the scattered radiation have

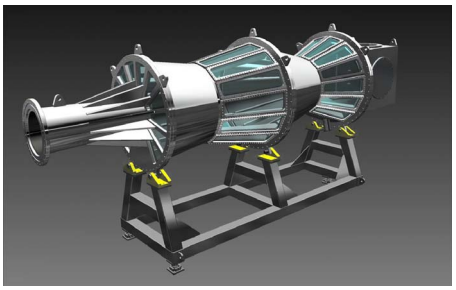

FIG. 5. (Color online) 3D rendering of the NIMROD sample and secondary flight path vacuum tank. This vacuum vessel provides a clean path for the neutrons scattered from the sample to the detectors.

been minimized. Each of the neutron windows of the vacuum tank that separate the vacuum from the face of the detector modules are constructed from 0.8-mm-thick aluminum sheets.

For standard experimental operations the sample point is accessed from above through a circular opening of 40 cm diameter, the ISIS standard. The flange plate that closes this aperture is positioned 30 cm above the center of the neutron beam. By adopting this standard size and relative position of the access point, NIMROD can benefit from the large pool of sample environment equipment available at ISIS. This includes cryostats for operations between 4 and 300 K, closed cycle refrigerators for temperatures between 10 and 320 K, furnaces for temperatures between 473 and 1373 K, and an automatic sample changer with 15 positions that operates at temperatures between 250 and 373 K. A second automatic sample changer that can operate down to cryogenic temperatures $(1-N_2)$ is currently under development. In addition to these standard pieces of sample environment equipment, ISIS also provides a range of NIMROD compatible sample cells that can operate from atmospheric to high pressures of ~5 kbar, as well as various sample environment setups for *in situ* gas and liquid handling experiments.

To further enhance the performance of the vacuum tank to provide a clean measure of the neutrons scattered by the sample, a set of boron carbide coated (1-cm-thick B_4C coating) collimating vanes are fitted inside each section of the vacuum tank and Fig. 7 shows a set of these collimating vanes. These vanes reduce the risk of increased background in the measured scattering signals by preventing scattering events from being detected in a detector module that arise from secondary scattering from adjacent aluminum windows

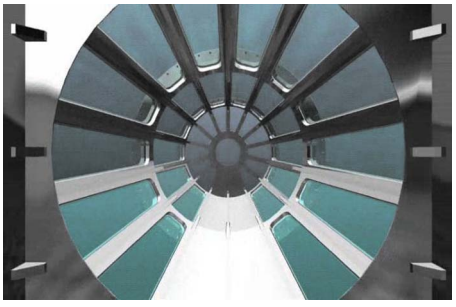

FIG. 6. (Color online) Illustration of the large solid angle of forward scattering detector coverage visible from the sample position.

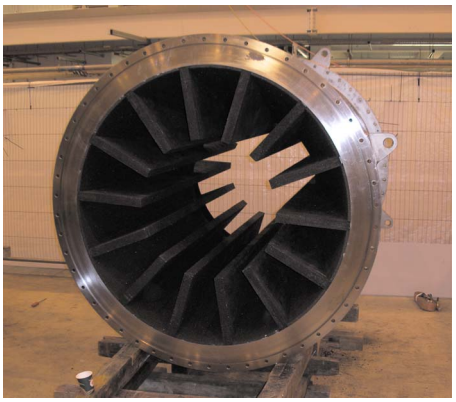

FIG. 7. (Color online) Photograph showing the internal collimation fitted within one section of the NIMROD vacuum tank.

of the vacuum tank. The vanes are designed to allow the detector modules to view the center of the sample plus or minus 20 cm. This generous view of the near sample area is to ensure that complex sample environment equipment can be used without the risk of inducing sample dependent background terms in the detector array due to differing views of the local scattering environment that arise in highly collimated detector configurations.

D. Detector array

The detector array and supporting data acquisition electronics (DAE) system are central to the performance and capabilities of the instrument. The wider angle array, covering scattering angles (2θ) from 3.5° to 40°, is constructed from 61 detector modules, each consisting of 18 detector elements arranged on a cylindrical surface of radius 70 cm about the neutron beam axis. Each scintillating element is formed from a multilayer sandwich of 23 layers of glass and 22 layers of ^{6}LiF dispersed in a matrix of Ag doped ZnS.[8–10] Each element is then viewed by two photomultiplier tubes configured within the detector electronics to operate in a coincidence counting mode. These elements operate as neutron detectors via the ^{6}Li (n,α) reaction.[11] The total size of the active face of an element is 1 cm (width) $\times$ 2 cm (depth) $\times$ 20 cm (height) and within each detector module the elements are angled to face the sample position. Figure 8 shows an exploded view of the components that form a wide angle detector module.

The NIMROD low angle detector bank is also based on ZnS (Ag) scintillation technology, and is a position sensitive dartboard style detector covering the scattering angle range from 0.5° to 2.2°. The detector face is split into 24 segments around the beam axis. To allow for the rectangular view of the moderator and associated difference in the horizontal and vertical beam divergence, the segments in the horizontal plane contain 30 radial elements while the segments in the vertical plane contain 33, all arranged with a 5 mm pitch. This gives 756 elements in total that are fiber coupled to 120 photomultiplier tubes, and that are coded in the detector electronics to allow each element to operate independently. Figure 9(a) shows the array of fiber optics that couples the packs of neutron scintillator to the photomultiplier tubes of the low

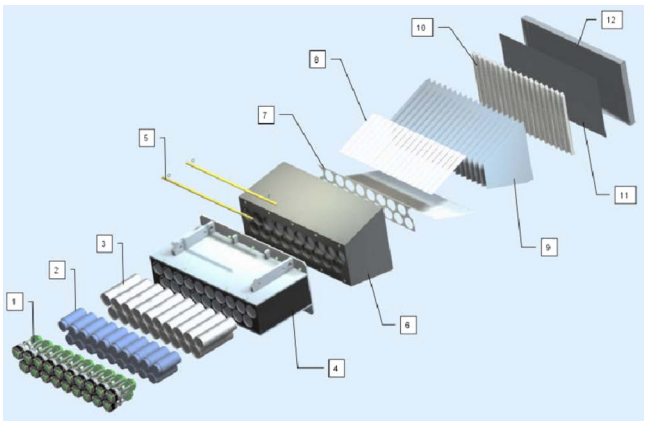

FIG. 8. (Color online) Exploded view of the components that form a NIMROD wide angle detector module. The components are (1) electronics assemblies; (2) photomultiplier tubes; (3) mu-metal assemblies for magnetic screening; (4) upper molding; (5) mounting pins; (6) lower molding; (7) upper reflective layer (8) reflector backing plates; (9) dividing plates; (10) glass and scintillator assemblies; (11) foil lining; and (12) detector cover.

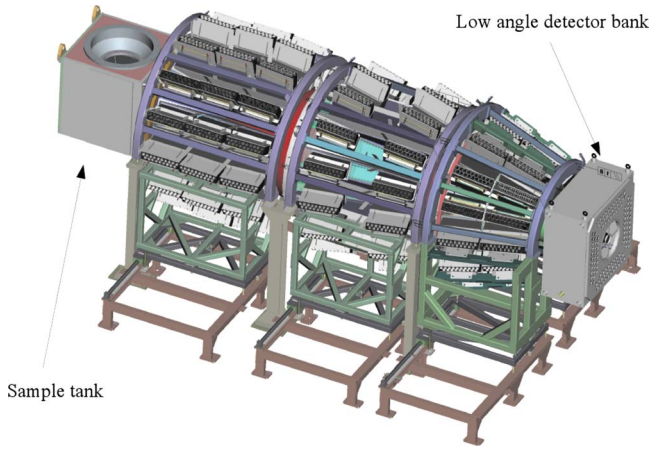

FIG. 10. (Color online) Overview of the distribution of the full complement of detector modules that can be mounted on NIMROD. The wide angle detector modules can be seen to be mounted in seven rings around the beam axis with the corresponding ranges in scattering angle 2θ given in Table I. A maximum of 12 modules can be mounted around each ring.

angle detector bank, while Fig. 9(b) shows the arrangement of the 24 detector segments mounted over the fibers. The fiber coupling of the low angle scintillation elements to the photomultiplier tubes allows them to be located inside the sample and secondary flight path vacuum tank. This minimizes the exposure of these elements to small angle background scattering that is unavoidably generated by vacuum and neutron window materials.

Figure 10 shows the design of the completed array of detector modules mounted around the instrument's sample and secondary flight path vacuum vessel. The design allows for a maximum of 84 detector modules in the wide angle positions, plus the low angle detector module. As reported above, the current instrument configuration consists of 61 wide angle modules plus the low angle bank. The distribution of detectors is summarized in Table I.

In total, NIMROD currently has 1854 detector elements. The standard grouping of the detector modules is to sum the counts in the detector elements around the beam axis corresponding to their position in the scattering angle. Effectively, this integrates the counts around the Debye–Scherrer scattering cones and improves the statistical quality of the output data. However, as each detector element can be probed individually, more complex detector groupings can be constructed that can better match their distribution in the data analysis to the requirements of specific sample geometries.

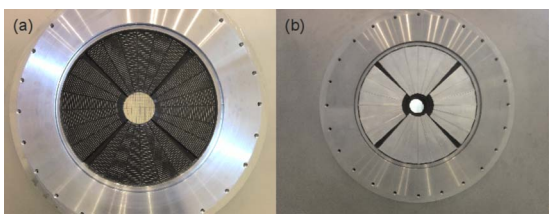

FIG. 9. (Color online) Photographs of the active face of the NIMROD low angle detector bank; (a) shows the array of fiber optics that connects the neutron scintillation elements to the banks of photomultiplier tubes and (b) shows the 24 segments of the neutron scintillation material mounted over the fiber optic array.

This effectively allows texture and preferred orientation in a scattering pattern to be investigated if desired.

The signals of the detector elements are processed using the ISIS DAE-II detector electronics system. This is the next generation of the original ISIS data acquisition electronics,[12] upgraded to be able to deal with larger numbers of detectors and increased numbers of time channels. Considerable care has been taken to ensure that the detector electronics are not subject to spurious sources of electronic interference or thermal drift. To achieve this, all the racks of detector and data acquisition electronic equipment are contained within an electrically shielded and thermally stabilized room, powered from a smoothed and filtered uninterruptible power supply and grounded to a single earthing point. All the power and signal cables that run between the electronics enclosure and the detectors in the instrument blockhouse are multiply screened and enclosed in sealed cable trunking for the full length of the cable run.

E. Detector blockhouse

The instrument blockhouse is constructed from wax filled steel tanks and houses the sample and secondary flight path vacuum tank and the array of detector modules. The walls of the blockhouse have a total thickness of 30 cm and serve to shield the detector array from any background radiation that does not arise from within the instrument as well

TABLE I. Angular ranges and distribution of the current number of detector modules and corresponding numbers of detector elements on NIMROD.

Angular range	Number of modules	Number of elements
0.5°–2.2°	24	756
3.5°–5°	4	72
6°–8°	2	36
9°–11°	9	162
12°–15°	10	180
18°–22°	12	216
24°–29°	12	216
31°–40°	12	216

as to protect people working around the instrument from any radiation scattered by the sample. The blockhouse itself is subject to both radiation and vacuum interlock systems to prevent any risk of human exposure to either of these hazards. As a core component of the scientific program envisaged for NIMROD involves isotope substitution experiments, an intrinsic stability of the detector array of better than $\pm 0.5\%$ is required. As the blockhouse houses the neutron detectors, its design incorporates a number of important environment controls to ensure stability of their performance. First, the blockhouse is temperature controlled to a stability of $\pm 1\ ^{\circ}\mathrm{C}$, and second, the atmosphere within the enclosure is humidity controlled to a relative humidity of $50 \pm 5\%$. This latter criterion is particularly important to ensure that the performance of the wide angle detector modules is consistent regardless of the prevailing weather conditions. For the wide angle detector modules that are furthest from the windows on the secondary flight path vacuum tank, the neutrons exiting the vacuum windows have a flight path through air of ~ 1 m before striking the active face of the detector. Fluctuations in relative humidity of more than 5%, would result in variations in the attenuation of the scattered beams of more than 0.1%. To ensure that the blockhouse environment controls are functioning reliably, extensive monitoring of the temperature and humidity around the instrument and detectors has been implemented.

F. Transmission monitor and beamstop

The final two components of the beamline are a transmission monitor and neutron beamstop. The transmission monitor is placed at the beam exit point of the blockhouse. This monitor is of similar construction to the incident beam monitors in the primary flight line that, as previously stated, are based on a thin vanadium scattering foil angled to scatter a fraction of the beam into a scintillator viewed by a photomultiplier tube. Information about the proportion of the neutron beam transmitted by a sample is particularly useful for performing basic diagnostics on issues such as sample composition.

The final element of the beamline is the neutron beamstop. This massive construct is formed from steel, concrete, and wax blocks.

III. PERFORMANCE

For a disordered materials and liquids diffractometer, one of the most useful quantities for characterizing performance is the count rate per Q-bin per unit volume of a standard scatterer, or C-number.[13] The almost completely incoherent scattering of vanadium and comparable scattering cross section to most elements (5.1 b) makes this material ideal for this purpose. The typical Q-bin used in studies of disordered materials and liquids has a width of 0.05 $\mathrm{Å}^{-1}$, so the units of the count rate are neutrons/s/0.05 $\mathrm{Å}^{-1}/\mathrm{cm}^3$ vanadium.

Once the C-number is known, it is possible to estimate the count rate that can be expected from a specific sample by multiplying the C-number by the volume of the sample and the ratio of the sample to vanadium scattering cross sections.

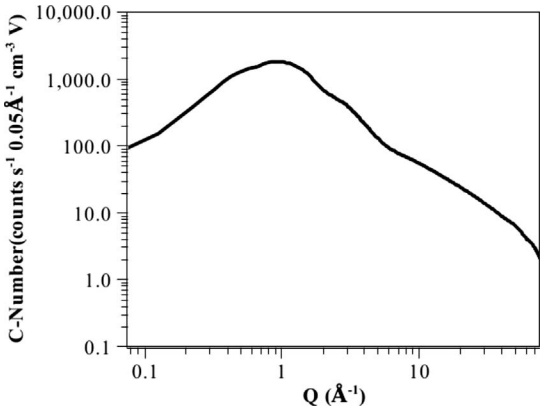

FIG. 11. The measured count rate for the NIMROD diffractometer under conditions where the ISIS second target station is operating at a proton beam current of 40 μA/h and the methane face of the coupled moderator is not filled.

Figure 11 shows the C-number measured for NIMROD when the ISIS second target station is operating with a proton beam current of 40 μA/h and with the methane face of the moderator unfilled.

The second quantity that is important for the characterization of a diffractometer is its resolving power.[13] For liquids and disordered materials type instruments, it is the Q-resolution that is the relevant quantity for consideration. As the scattering from noncrystalline materials does not give rise to many closely spaced sharp peaks in the structure factor, a resolution in the region of $\Delta Q/Q \approx 10^{-2}$ is adequate compared to the value of $\approx 10^{-3}$, which would generally be required for a powder crystallography instrument.

For time-of-flight instruments the resolution function is more or less a constant over the majority of the accessible Q-range. This is because the wide angle detector banks dominate and their Q-resolution is similar over a broad angular range. The Q-resolution at low angles unavoidably degrades due to the well known dependence of this function on cot θ which diverges as θ goes to zero. Figure 12 shows the resolution of NIMROD as a function of the angular position on the detector array. When using the full view of the mod-

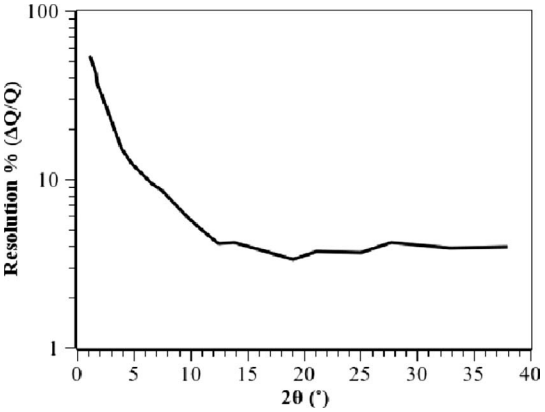

FIG. 12. Measured Q-resolution (FWHM) for the NIMROD diffractometer as a function of the angular position of the detector on the instrument's array. The view of the hydrogen moderator and water premoderator is 11.5 cm vertical by 19.5 cm horizontal, and the beam size at the sample position is 3×3 cm^2.

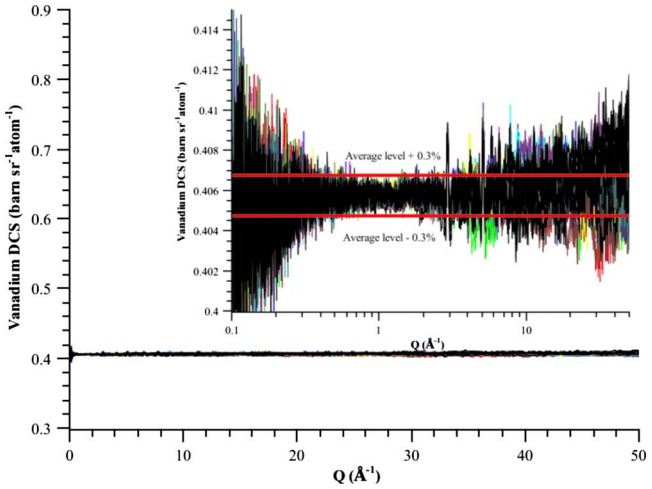

FIG. 13. (Color online) The differential scattering cross section for 19 consecutive 1 h measurements made for a vanadium standard sample on NIMROD, normalized to vanadium. The inset figure shows a zoomed image of the data highlighting the ±0.3% stability window. At the extremes of the Q-range the intrinsic statistics of the 1 h measurements limits our ability to clearly establish the detector stability in these regions. However, as all detector modules contribute to the region of highest statistical quality, the stability of the detector array itself is clearly better than ±0.3%.

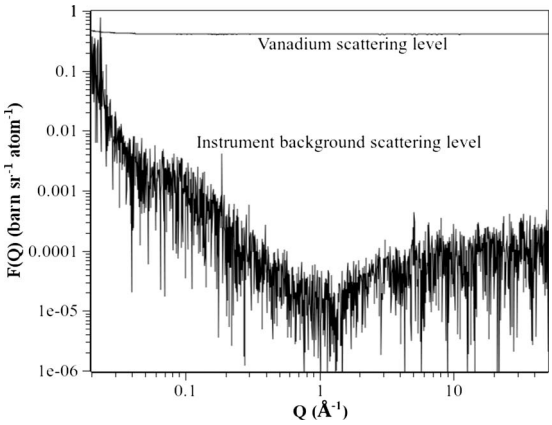

FIG. 14. The intrinsic background scattering contribution measured on NIMROD compared to the scattering of a standard vanadium sample.

erator and premoderator with the maximum beam size at the sample, above $Q \approx 0.5$ Å^{-1}, the Q-resolution of the instrument is ≈4%. At the expense of flux, this resolution can be improved within in a factor ~2 by making use of the variable collimation in the incident neutron flight path to limit the size and divergence of the primary beam.

As discussed in the description of the detector blockhouse, the third critical parameter for a liquids and disordered materials neutron diffractometer is the stability of the detector array. Isotopic substitution experiments require the ability to measure small difference functions between the structure factors of two or more samples that have identical atomic and molecular structures, but differ in the neutron scattering power of selected isotope labeled sites.[3] The magnitude of these differences in the total structural signals are often at a 1% level or less. Generally, the logistics of the experimental procedure require the structure factor measurements on each isotopic sample to be performed independently over a period of days. Each measurement needs several hours of data accumulation to achieve sufficient statistical quality to facilitate the technique and consequently the stability of the instrument is critical if spurious systematic errors are to be avoided in the difference data. To evaluate the stability of the NIMROD detector array, a series of 1 h measurements on a standard vanadium sample have been performed over a 20 h period. The comparison of the series of measurements is shown in Fig. 13, and the inset shows that where the 1 h counting statistics allow, and noting that all detector modules contribute to this region, the stability of the detector array is better than ±0.3%. Assuming that the outlying points reflect the 3σ standard deviation level, the intrinsic stability of the detector array can be estimated to be ~0.1%.

To complete the characterization of the instrument performance, a measure of the intrinsic background scattering contribution of NIMROD across its optimal Q-range is shown in Fig. 14. For most of the instrument's Q-range, the background contribution can be seen to be ~4 orders of magnitude smaller than the structure factor signals of interest. The rise in the background scattering contribution with decreasing Q reflects the proximity of the detector banks to the direct beam passing through the instrument, and the unavoidable background scattering contributions at low angles that arise from optical elements such as vacuum windows and collimation elements in the primary neutron flight line.

IV. BENCHMARK SAMPLES

To benchmark the performance of the instrument to investigate structure from atomic to nanometer length scales, a series of measurements have been performed on the amorphous silica system. Silica is the archetype of a strong glass where each silicon atom is covalently bonded in a tetrahedral geometry to four neighboring oxygen atoms. Each of these oxygen atoms is in turn bonded to a second silicon atom and the extended network structure of the material is formed from this basis. As a bulk glass, fused silica does not display any structural texture on the nanoscale, and is thus a good test for how accurately a wide Q-range diffractometer can measure a homogenous material on the longer length scales. In contrast, liquid crystal[14] and biomimetic[15] templating techniques, among others, have enabled the manufacture of silicate materials that are structured on nanometer length scales. Typical examples are the classic MCM (Ref. 14) and MSU (Ref. 15) type materials. These nanostructured materials are typically formed from ordered arrays of cylindrical pores on a crystalline lattice, with typical lattice constants in the 20–500 Å range. For the purposes of benchmarking the low-Q, large-r capabilities of NIMROD, three commercial grade mesostructured silicas were obtained from the Aldrich chemical company: (i) MCM-41, the classic ordered hexagonal lattice of pores with a lattice constant of ≈46 Å and an estimated pore size of 27 Å; (ii) mesostructured HMS-wormhole silica, a fumed silica with a disordered porous network structure with a characteristic length scale of ≈39 Å; and (iii) large pore MSU-H, an ordered mesostructured silica with a lattice constant of ≈116 Å and an esti-

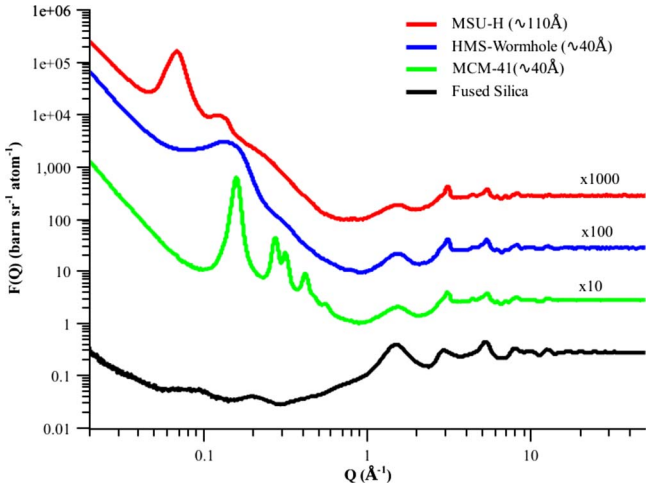

FIG. 15. (Color online) The differential cross sections of a series of silica glass samples measures on NIMROD. From bottom to top are (i) fused silica, (ii) MCM-41, (iii) HMS-wormhole, and (iv) MSU-H silica. For clarity of presentation and as the ordinate is presented on a logarithmic scale, the MCM-41, HMS-wormhole, and MSU-H functions have been multiplied by factors of 10, 100, and 1000, respectively.

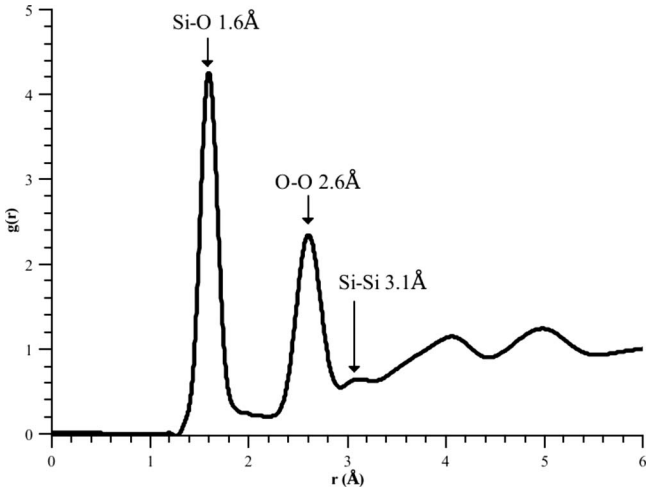

FIG. 16. The total pair distribution function $g(r)$ for the sample of fused silica measured on NIMROD. This function was obtained by the direct Fourier transform of the total structure factor shown in Fig. 15.

mated pore size of 71 Å. All of these materials have a silica-glass-like structure on the interatomic length scale.

The sample of fused silica glass was a self-supporting circular glass plate of 5.0 cm diameter and 0.3 cm thickness. The mesoporous silicas were powder samples that were contained in null-scattering TiZr alloy cells of 0.1 cm wall thickness and internal dimensions 3.5 cm (width) $\times$4.0 cm (height) $\times$0.2 cm (thickness). All measurements were made at room temperature using the instrument's 15 position automatic sample changer, and the data were corrected for instrument and container backgrounds, absorption, and multiple scattering, and were normalized to the scattering of a $5\times5\times0.3$ cm^3 thick vanadium plate using the Gudrun analysis routines. These are based on the algorithms outlined in the widely used Atlas package.[13]

Figure 15 shows the differential scattering cross section of the four samples measured on NIMROD. The intensity of the low-Q scattering of the fused silica sample is three orders of magnitude smaller than the scattering from the mesostructured materials. This reflects the structurally homogenous nature of the material on length scales beyond 1 nm. The small rise at the very lowest Q-values is believed to be a background scattering artifact, and shows the current limit of sensitivity of the instrument to small fluctuations on nanometric length scales. This limit corresponds to fluctuations of approximately 1 atom in 1000 atoms on a 30 nm length scale. In comparison, the small angle scattering of the mesostructured materials rises to a cross section of several hundred barns sr^{-1} atom^{-1} at the measured low-Q limit of 0.02 Å^{-1}. The general rise in the scattering as the functions progress to lower-Q reflects the Porod scattering[16] behavior of a nanometrically inhomogenous material, while the peaks at low-Q reflect the length scale of the characteristic mesostructure of the materials.

The oscillations in the differential scattering cross section above $Q\approx0.5$ Å^{-1} contain the information about the short and intermediate range chemical structure of the material. Figure 16 shows the direct Fourier transform to $g(r)$ of the data from the fused silica sample on the short range interatomic length scale. This function clearly shows the expected features of the local chemical order,[17] i.e., the Si–O first neighbor correlation at 1.6 Å, the O–O first neighbor correlation at 2.6 Å, and the Si–O–Si correlation at 3.1 Å. To further confirm the quantitative nature of the data, the integral of the Si–O peak between 1.3 Å$\leq r\leq$2.1 Å corresponds to 4.0 (1) oxygen atoms around each silicon atom, while the integral of the O–O peak between 2.1 Å$\leq r\leq$2.9 Å corresponds to 6.1 (1) oxygen atoms around each oxygen atom, as expected for this material.

The leading peak in the MCM-41 $F(Q)$ occurs at a position of 0.16 Å^{-1} which corresponds to a length scale of $\approx$40 Å. The first peak in the HMS-wormhole $F(Q)$ also peaks close to this value, but the difference in the ordering of the nanoscale structure makes the features quite different. The disorder in the HMS-wormhole material leads to the lack of significant higher-order features in the low-Q region of its $F(Q)$ and the increased width of the principle peak. The pore structure of the MSU-H material clearly occurs on a much larger length scale than the MCM-41 or HMS-wormhole systems, with the leading feature in $F(Q)$ occurring at a position of $\approx$0.07 Å^{-1}. To illustrate the capability of NIMROD to characterize this nanoscale structural texture, Fig. 17 shows the differential pair correlation functions $D(r)$ obtained by Fourier transform of the $F(Q)$ data.

The $D(r)$ clearly show the difference in the nanoscale structure between the ordered MCM-41 and MSU-H samples and the disordered HMS-wormhole silica. The regular lattice of the former materials is seen in the high-r features that are periodic in the leading length scale of the nanostructure. In the porous silica systems this length scale is governed by the correlation length between the regions of silica between the pores, since neutrons scatter from the atoms and not the free space. The leading length scales of the silica correlations in MCM-41, HMS-wormhole, and MSU-H silicas are thus $\approx$48, $\approx$50, and $\approx$110 Å. The disordered nature of the mesostructure of the HMS-wormhole sample is clearly seen as a

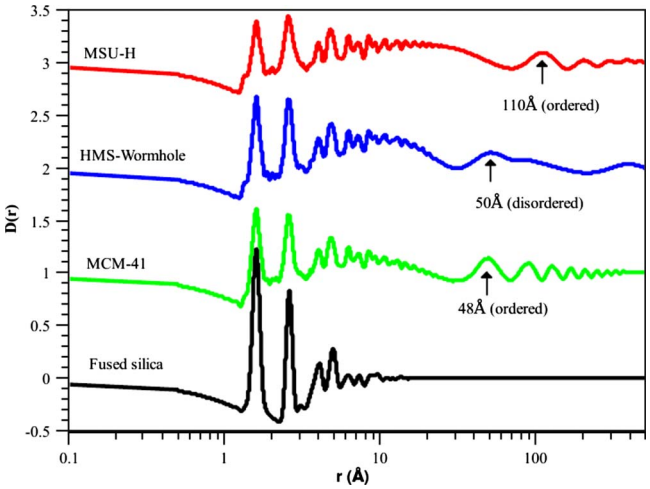

FIG. 17. (Color online) The differential pair correlation functions, from bottom to top, of (i) Fused silica, (ii) MCM-41 silica, (iii) HMS-wormhole silica, and (iv) MSU-H silica. The $D(r)$ for MCM-41, HMS-wormhole, and MSU-H silica have been offset vertically by 1.0, 2.0, and 3.0 units, respectively.

very broad range of structural correlations in the 30–100 Å range, as opposed to a series of period structural correlations. The lack of any nanoscale structural features in the fused silica sample confirms the ability of the NIMROD to measure structurally homogenous materials without introducing structural artifacts into the long range *r*-space data.

V. FUTURE UPGRADE OPTIONS

Due to the limitations of a finite budget during the build phase of the instrument, various technical options that were conceived during its design were moved to a future upgrade status. These upgrade options include:

1. Completion of the wide angle detector array by increasing the number of detector modules from 61 to 84 in the $2\theta=3.5°$ to 40° range. The addition of these extra modules would provide an improvement in the instrument count rate in the important intermediate Q-range from 1 to 10 $Å^{-1}$.
2. Installation of a T_0 chopper to reduce the neutron and gamma-ray background levels immediately after each pulse of protons from the ISIS accelerator impacts the target.
3. Installation of a Fermi chopper to allow the instrument to perform low-resolution inelastic scattering measurements.[18]
4. Installation of a wider angle detector bank $2\theta=60°$ to 90° to facilitate higher resolution ($\Delta Q/Q \approx 0.6\%$) measurements in the higher Q-range for samples that do not contain hydrogen.

VI. SCIENTIFIC PROSPECTS AND OUTSTANDING CHALLENGES

NIMROD received its first neutrons at 8:30 pm on Wednesday, 10 December 2008, and all commissioning tests to date have confirmed that the instrument has delivered or exceeded its originally envisaged key performance criteria. Under the current operating conditions of the ISIS second target station, NIMROD routinely allows access to its mission critical Q-range of 0.02–50.0 $Å^{-1}$ and excitingly, its operational performance is expected to improve further as the optimization of the target station's target and moderator assembly is continued.

The ability to quantitatively study the structure of liquids and modern materials on a continuous length scale from the atomic to the nanometric raises many new opportunities for improving our understanding of important growth areas of modern pure and applied science. A nonexhaustive list of examples includes the investigation of (i) biomolecules in solution, where the intrinsic size of small proteins is well matched to the nanoscale capabilities of the instrument; (ii) confined fluids, where the phase behavior of liquids can be modified to allow the investigation of deeply supercooled states; and (iii) porous media and intercalates that are key substrates for a growing amount of catalytic chemistry and energy storage issues such as hydrogen sequestration.

The novel ability of the instrument to obtain quantitative structural information with atomic precision to length scales of ≈30 nm inevitably brings some new challenges to our conventional approaches for data analysis.[19–21] In almost every area of modern condensed matter science, classical and quantum atomistic simulations have played an immense role in advancing our understanding. The challenge NIMROD brings is the requirement for atomistic models to be built and refined that contain millions of atoms. Current desktop computational facilities can typically manage systems with up to 250 000 atoms. As an example, considering the structure of pure water on a length scale of 30 nm would require a simulation to be performed on a system of at least 60 nm in size. At this length scale, the model would need to contain 21.6×10^6 atoms! As the experimental data have subatomic resolution for distances and atomic resolution for molecular form and texture, current coarse graining approaches that are increasingly being used to perform large scale simulations[22] are not immediately suitable. Further innovation continues to be required.

[1] A. K. Soper, Mol. Phys. **107**, 1667 (2009).
[2] D. T. Bowron, J. Phys.: Conf. Ser. **190**, 012022 (2009).
[3] J. L. Finney and A. K. Soper, Chem. Soc. Rev. **23**, 1 (1994).
[4] V. F. Sears, Neutron News **3**, 26 (1992).
[5] D. A. Keen, J. Appl. Crystallogr. **34**, 172 (2001).
[6] Nimonic alloy 75, ~70% Ni, ~20% Cr, ~5% Fe, and balance (C, Cu, Mn, Si, and Ti).
[7] GS20 glass scintillator is formed from an aluminosilicate glass containing ~18 wt % Li_2O (95% ^6Li), doped with Ce.
[8] F. Mantler-Niederstätter, F. Bensch, and F. Grass, Nucl. Instrum. Methods **142**, 463 (1977).
[9] M. Katagiri, K. Sakasai, M. Matsubayashi, T. Nakamura, Y. Kondo, Y. Chujo, H. Nanto, and T. Kojima, Nucl. Instrum. Methods Phys. Res. A **529**, 274 (2004).
[10] N. J. Rhodes, Neutron News **17**, 16 (2006).
[11] G. F. Knoll, *Radiation Detection and Measurement*, 3rd ed. (Wiley, New York, 2000).
[12] S. Quinton, M. Johnson, J. Norris, W. Pulford, and M. Watt, IEEE Trans. Nucl. Sci. **37**, 2156 (1990).
[13] A. K. Soper, W. S. Howells, and A. C. Hannon, "ATLAS analysis of time-of-flight diffraction data from liquid and amorphous samples," Rutherford Appleton Laboratory Report No. RAL-89–046 (Oxfordshire, United Kingdom, 1989).

[14] C. T. Kresge, M. E. Leonowicz, W. J. Roth, J. C. Vartuli, and J. S. Beck, Nature (London) **359**, 710 (1992).
[15] P. T. Tanev and T. J. Pinnavaia, Science **271**, 1267 (1996).
[16] L. A. Feigin and D. I. Svergun, *Structure Analysis by Small-Angle X-ray and Neutron Scattering* (Plenum, New York, 1987).
[17] D. T. Bowron, Mater. Sci. Eng., B **149**, 166 (2008).
[18] A. Botti, M. A. Ricci, D. T. Bowron, and A. K. Soper, Physica B **385–386**, 1070 (2006).
[19] A. K. Soper, Chem. Phys. **202**, 295 (1996).
[20] A. K. Soper, Phys. Rev. B **72**, 104204 (2005).
[21] R. L. McGreevy, J. Phys.: Condens. Matter **13**, R877 (2001).
[22] C. Peter and K. Kremer, Faraday Discuss. **144**, 9 (2009).

Review of Scientific Instruments is copyrighted by the American Institute of Physics (AIP). Redistribution of journal material is subject to the AIP online journal license and/or AIP copyright. For more information, see http://ojps.aip.org/rsio/rsicr.jsp